Method for determining effective nonradiative lifetime and leakage losses in double-heterostructure lasers

C. van Opdorp and G. W. 't Hooft

Citation: Journal of Applied Physics **52**, 3827 (1981); doi: 10.1063/1.329845
View online: http://dx.doi.org/10.1063/1.329845
View Table of Contents: http://scitation.aip.org/content/aip/journal/jap/52/6?ver=pdfcov
Published by the AIP Publishing

Method for determining effective nonradiative lifetime and leakage losses in double-heterostructure lasers

C. van Opdorp and G. W. 't Hooft
Philips Research Laboratories, Eindhoven, The Netherlands

(Received 10 October 1980; accepted for publication 25 February 1981)

Carrier losses in double-heterostructure lasers are twofold: (i) nonradiative recombination through killers in the bulk of the active region and at all its boundaries (interfaces and surfaces), and (ii) leakage out of the active region. A simple theory shows the following. In the high-injection regime ($p \simeq n$) all processes under (i) are directly proportional to n. Consequently their contributions can be lumped together in a single effective nonradiative carrier lifetime τ_{nr}; this τ_{nr} is constant (i.e., independent of n) owing to the constant degree of occupation of all killers in the mentioned regime. On the other hand, the leakage losses (ii) are superlinear in n. This provides a well-grounded basis for disentangling the contributions of (i) and (ii) in a given sample. Further, a simple method is presented for accurately determining τ_{nr} from data of the external quantum efficiency η_{ext} measured as a function of current I in the spontaneous high-injection regime below the laser threshold. Knowledge of the light-extraction factor (i.e., the ratio of external and internal quantum efficiencies) is essentially unnecessary with this method. However, optionally it can be determined easily from a slight extension of the method. For illustration the method of determining τ_{nr}, which is also applicable to double-hetero LED's, has been applied to some thirty LPE and metal-organic VPE GaAs-(Ga,Al)As lasers of widely varying qualities. The values found vary between 0.8 and 55 ns. From the measured values of τ_{nr} it follows that the upper limit for the interface recombination velocity in the best samples is 270 cm/s. For most samples τ_{nr} cannot account for all electrical losses at laser threshold. The superlinear "excess" losses are ascribable to leakage.

PACS numbers: 42.55.Px, 72.20.Jv, 85.60.Jb

I. INTRODUCTION

We shall consider double-heterostructure lasers with a well-defined volume of the active region (broad-area and high-mesa structures) so that no current-spreading effects occur. Only the following types of carrier losses can occur in such samples: (i) recombination losses through killers situated in the bulk of the active region and through killers situated at any of its boundary planes (interfaces with cladding layers, and outer surfaces); and (ii) leakage of carriers from the active layer into one or both cladding layers and subsequent recombination there.

In general the disentanglement of carrier losses into these two types of losses is difficult. We shall show, however, that in the spontaneous high-injection regime of lasers with undoped or moderately doped active layers (so that $p \simeq n \gg N$) the situation becomes much simpler. The crucial point is that all losses of type (i) can be shown to be directly proportional to n in this regime. This means that all these losses can be lumped together in a single overall proportionality constant, or in a single effective nonradiative carrier lifetime τ_{nr} which is independent of n. On the other hand, the type (ii) or leakage losses, which are due to thermal emission and tunneling (and subsequent recombination), will be shown to be superlinear in n. This characteristic difference provides a well-grounded basis for disentangling the type (i) and type (ii) losses in a given sample.

It will turn out that over the larger part of the spontaneous high-injection interval the type (i) losses dominate the leakage losses. This is the case even in samples where leakage losses dominate at laser threshold owing to their superlinearity versus the linearity of the type (i) losses. It will be shown that this circumstance allows a very accurate evaluation of τ_{nr} from measurements of the external quantum efficiency η_{ext} as a function of current I in the spontaneous emission regime.

Our method of evaluating τ_{nr} consists of a special way of processing these data. The essentials are (a) a simple but adequate model for describing the expected dependence of η_{ext} on I, and (b) plotting the experimental data in such a way that according to the model they should lie on a straight line. This provides an easy check on the validity of the model, as well as an easy and accurate method of evaluating τ_{nr}.

Once τ_{nr} is known, the type (i) losses at threshold can be estimated with ample accuracy. The "excess" carrier losses contributing to the measured laser threshold current are ascribable then to leakage.

In Sec. II the theory of the type (i) and (ii) losses is presented, together with the method of evaluating τ_{nr} from efficiency measurements. In Sec. III information is given on the measuring apparatus and on a number of samples investigated for illustrating the method. Results and discussion follow in Sec. IV. In Sec. V our method of determining τ_{nr} is compared with alternative approaches in the literature. The conclusions are given in Sec. VI.

II. THEORETICAL CONSIDERATIONS

In this section the theory of the type (i) and (ii) losses is given. In Sec. II A we present the model which predicts that

 0021-8979/81/063827-13$01.10

for $p \simeq n \gg N$ all type (i) losses are directly proportional to n. In Sec. II B the method of evaluating τ_{nr} is presented. The expected superlinearity of the type (ii) or leakage losses with n is treated in Sec. II C.

A. Type (i) or linear losses

The following assumptions will be made.

(1) The volume V of the active region is well defined and current independent. Ideally this can only be achieved in broad-area and high-mesa samples. In the cladding layers of such samples there is no current spreading; after injection the carriers can only recombine in the active volume and at its boundary planes.

(2) The net ionized dope concentration N in the active region is considerably lower than the injected carrier concentrations near laser threshold (i.e., $N \ll 2 \times 10^{18}/\text{cm}^3$).[1,2] In these cases there will be a more or less extended high-injection regime below this threshold where $p \simeq n \gg N$.

(3) In the high-injection regime the mobile carrier concentrations in the active region are homogeneous. This sets an upper limit to s_1 and s_2.[3] Further the dimensions of the active region should fulfill the condition $d \ll L_{amb} \ll \frac{1}{2}b$, where L_{amb} is the ambipolar diffusion length. If $d \ll L_{amb}$, there are practically no concentration variations perpendicular to the interfaces. If $L_{amb} \ll \frac{1}{2}b$, the widths of the layers of reduced concentration adjoining the outer surfaces (due to surface recombination) are negligible. In Appendix A these conditions for homogeneous carrier concentrations are considered in more detail. In practice they turn out to be easily fulfilled.

The type (i) losses consist then of the following three contributions.

(a) Recombination through bulk killers. In stationary state the recombination rate through an individual center is given by $K' = pc_h f = nc_e(1-f)$, when thermal emission is neglected. In this equation c_h and c_e are the capture coefficients for holes and electrons, while f is the probability of occupation by an electron. For $p = n$, the equation yields a concentration independent occupation $f_0 = (1 + c_h/c_e)^{-1}$. This corresponds to the state of complete "saturation" of the killer center. Substituting the expression for f_0 back in the equation for K' one finds for the recombination rate through a single killer center:

$$K' = n(1/c_h + 1/c_e)^{-1}. \tag{1}$$

The above argumentation can easily be generalized by taking into account thermal reemission from the killers. It turns out then that for any killer energy depth the reemission becomes negligible in the $p \simeq n$ regime, so that Eq. (1) remains valid here.[4]

Equation (1) expresses the linear dependence of K' on n for any individual killer center. The total recombination rate through all bulk killers in the active region K_b is found from the addition of all individual contributions K'. This yields a linear dependence of K_b on n, including cases of inhomogeneous killer distributions and/or the presence of different types of killers. In the simplest case of a homogeneous distribution of a single type of killer center with density N_k the addition yields

$$K_b = Vn/\tau_{nr}^b, \tag{2}$$

where the constant saturated nonradiative bulk lifetime τ_{nr}^b equals

$$\tau_{nr}^b = 1/N_k c_h + 1/N_k c_e \equiv \tau_h^b + \tau_e^b. \tag{3}$$

In the following we shall make use of the simple equations (2) and (3) exclusively. If necessary, the lifetimes figuring in these equations should be considered as proper averages over different types of killers and over inhomogeneous distributions.

(b) Recombination at the interfaces. Owing to the carrier density homogeneity, the condition $p \simeq n$ also prevails at both interfaces. Therefore the treatment of recombination through interface killers proceeds in complete analogy with that through bulk killers. Consequently their occupation is also invariant here, leading to constant "saturated" recombination velocities s_1 and s_2. Thus the recombination rate at both interfaces equals

$$K_i = bln(s_1 + s_2), \tag{4}$$

where s_1 and s_2 are constant, saturated interface recombination velocities.

(c) Recombination at the outer surfaces. In contrast with the interfaces (see Appendix A) near the outer surfaces a layer of reduced carrier concentrations may be present. In spite of this, the recombination rate per unit of surface area may still be written formally as nv.[5] Here v stands for

$$v \equiv (1/s_s + 1/v_{diff})^{-1}, \tag{5}$$

where $v_{diff} \equiv (2D_h/\tau^b)^{1/2}$, with $1/\tau^b = 1/\tau_r + 1/\tau_{nr}^b$ while s_s is the surface-recombination velocity. Thus the recombination rate at the surfaces equals[6]

$$K_s = 2d(b + l)nv. \tag{6}$$

The total type (i) losses K are found by adding Eqs. (2), (4), and (6). This yields finally the direct proportionality to n:

$$K = Vn/\tau_{nr}, \tag{7}$$

where

$$\frac{1}{\tau_{nr}} = \frac{1}{\tau_{nr}^b} + \frac{s_1 + s_2}{d} + 2\left(\frac{1}{b} + \frac{1}{l}\right)v. \tag{8}$$

B. The method of evaluating τ_{nr}

We shall develop now our method of evaluating τ_{nr} from efficiency measurements. The internal quantum efficiency η is, by definition

$$\eta \equiv qL/I. \tag{9}$$

Here L is the total photon generation rate in the active region, and I is the electrical current through the device.

Under the assumptions (1)–(3) at the beginning of Sec. II A, in the spontaneous high-injection regime L will be given by[7]

$$L = BVn^2. \tag{10}$$

Let us consider further the case that in this regime leakage losses are negligible. In Sec. II C we shall extend the model so

as to include leakage losses. The current I is now given by

$$I/q = L + K. \tag{11}$$

From Eqs. (9) and (11), with the aid of Eqs. (7) and (10), it follows that

$$\frac{1}{\eta} = 1 + \frac{K}{L} = 1 + \frac{1}{Bn\tau_{nr}}. \tag{12}$$

In this equation we can express n in L through Eq. (10):

$$\frac{1}{\eta} = 1 + \frac{1}{\tau_{nr}}\left(\frac{V}{BL}\right)^{1/2}. \tag{13}$$

Thus plotting of experimental data in a $1/\eta$ vs $1/\sqrt{L}$ plot would result in a straight line from whose slope τ_{nr} could be evaluated (assuming that the value of B is known). However, in order to make such a plot one has to know the reduction factor $C\,(<1)$ between the externally measured value L_{ext} and the internal L; obviously the same factor figures between the measured and internal values $\eta_{ext}\,(\equiv qL_{ext}/I)$ and η:

$$L_{ext}/L = \eta_{ext}/\eta = C. \tag{14}$$

In the spontaneous high-injection regime the factor C of a given sample will be constant (independent of n) if two conditions are fulfilled:

(1) The layers of reduced carrier concentrations adjoining the outer surfaces do not contribute appreciably to L_{ext}. This is always the case since the local efficiencies in these layers are lower than in the bulk, and the absorption length of the emitted light $1/\alpha$ is large compared to L_{amb} ($1/\alpha$ is of the order of some tens of μm, whereas the upper limit of L_{amb} is a few μm, cf. Appendix A).

(2) The absorbed fraction of the spontaneous light generated at a given point in the bulk is independent of n. For increasing n the spectral absorption curve shifts to higher photon energies, owing to considerable occupation of the lower energy levels when the electron quasi-Fermi level comes close to the conduction-band minimum[10,11] (Burstein shift). This is accompanied, however, by a similar shift of the spontaneous emission curve, brought about by the same cause. Though an exact analysis has not been made, qualitatively these two effects may be expected to result in an extension of the range of constant C beyond the concentration where the mentioned spectral shifts show up.[12]

Accurate determination of the reduction factor C is generally very difficult. In our approach this is accomplished in a very simple way from a plot of $1/\eta_{ext}$ vs $1/\sqrt{L_{ext}}$. Substituting Eq. (14) in (13) we obtain

$$\frac{1}{\eta_{ext}} = \frac{1}{C} + \frac{1}{\tau_{nr}}\left(\frac{V}{CBL_{ext}}\right)^{1/2}. \tag{15}$$

Plotting the experimental data in a $1/\eta_{ext}$ vs $1/\sqrt{L_{ext}}$ plot will yield a straight-line interval for the regime considered if our assumptions of a constant factor C and negligible leakage current are correct. Extrapolating this straight line to $1/\sqrt{L_{ext}} = 0$ yields the value of C. Using this value, τ_{nr} can be calculated from the slope of the straight line:

$$\tau_{nr} = \left(\frac{V}{CB}\right)^{1/2}\frac{\Delta\,(1/\sqrt{L_{ext}})}{\Delta\,(1/\eta_{ext})}. \tag{16}$$

The gist of the above determination of C is that—according to Eq. (14)—η_{ext} equals C for the case of $\eta = 100\%$. For any sample this hypothetical case corresponds to infinite values of n [Eq. (12)], L [Eq. (10)], and thus of L_{ext} [Eq. (14)]. Optionally, once C is known, all measured values of η_{ext} might be transformed to internal-efficiency values η.

With respect to the factor C the following is further noteworthy. Suppose L_{ext} is expressed as the electron flux in the photodetector circuit of the measuring equipment (and η_{ext} consequently as the ratio of the electron fluxes through the photodetector and through the sample). The reduction factor C then equals the product of the following three factors: the light-extraction factor or average photon escape probability C_{extr} (accounting for the internal losses in the sample due to absorption), the transfer efficiency of emitted photons to reach the detector surface (a geometrical factor), and the detector efficiency. It is obvious that in our method we need not bother about optimizing or even knowing any of these factors separately. However, frequently (though not in the problems treated in this paper) one wants to know the value of the light-extraction factor C_{extr}, which is the only device-determined factor. Since the product of the other two (apparatus-determined) factors can easily be found by calibrating, our method of evaluating C can also be considered as a possible simple means of accurately determining C_{extr}.

For our purpose, L_{ext} may be expressed in completely arbitrary units, provided the same units are used for calculating $\eta_{ext}\,(\equiv qL_{ext}/I)$.

C. Type (ii) or superlinear losses

In this section it will be shown that the type (ii) or leakage losses are superlinear in n. To be specific we shall consider a GaAs-(Ga,Al)As laser; the conclusions are not restricted, however, to this specific case.

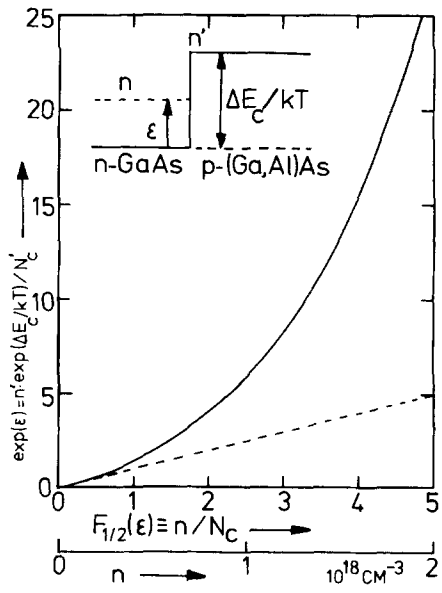

FIG. 1. Normalized electron density in confinement layer in units $\exp(-\Delta E_c/kT)$ vs normalized electron density in the active layer; the bottom scale along the abscissa gives absolute values for the case of GaAs ($N_c = 4\times 10^{17}/\mathrm{cm}^3$). The broken line represents the Boltzmann approximation. In the inset the electron quasi-Fermi energy ϵ (in units kT) is shown.

The main source of leakage is the escape of electrons to the p(Ga,Al)As layer.[14] This escape proceeds by way of thermal emission into the (Ga,Al)As conduction band, followed by diffusion and recombination there (and possibly in the p GaAs top layer). In this series of processes the diffusion is rate determining. Thus the leakage flux equals the product of the electron density n' in the (Ga,Al)As near the interface and the diffusion velocity $v'_{\rm diff}$ with which these electrons move further into the (Ga,Al)As layer.

For the following it is assumed that in the high-injection regime the potential drops still remaining on either side of the interface are negligible. The resulting flat-band situation of the conduction-band edge near the interface is schematically given in the inset of Fig. 1. This simplified model can be expected to exhibit the essential features of the superlinearity in a simple, perspicuous way.

For a discontinuity ΔE_c in the conduction-band edge, n' at the interface is given by

$$n' = N'_c \exp(-\Delta E_c/kT)\exp(\epsilon). \tag{17}$$

Here N'_c is the effective density of states in the (Ga,Al)As conduction band; ϵ equals the difference between the electron quasi-Fermi energy and the bottom of the GaAs conduction band, expressed in units kT (see inset of Fig. 1). Now we want to express n' in n, the electron density in the active layer. The latter is given by

$$n = N_c F_{1/2}(\epsilon), \tag{18}$$

where $F_{1/2}$ is the Fermi-Dirac integral of order $\frac{1}{2}$. Elimination of ϵ from Eqs. (17) and (18) will yield the relation between n' and n. This is done in Fig. 1 by plotting $\exp(\epsilon)$ vs $F_{1/2}(\epsilon)$; this is identical to a normalized plot of $(n'/N'_c)\exp(\Delta E_c/kT)$ vs n/N_c. This plot shows a strong superlinearity between n' and n, which will be reflected in the dependence of the leakage losses $n'v'_{\rm diff}$ on n.

For $n/N_c < 0.5$ the curve of Fig. 1 can be approximated by a straight line. Actually this is the interval where Eq. (18) can be represented adequately by the Boltzmann expression

$$n = N_c \exp(\epsilon). \tag{19}$$

Substitution of Eq. (19) in (17) yields a linear relation between n' and n in this interval. The corresponding expression for the leakage current density $J_l^{\rm lin}$ is also linear in n if $v'_{\rm diff}$ is independent of n[15]:

$$\frac{J_l^{\rm lin}}{q} = n'v'_{\rm diff} \simeq n\left(\frac{N'_c}{N_c}\right)\exp\left(\frac{-\Delta E_c}{kT}\right)v'_{\rm diff}. \tag{20}$$

The concentration interval in which this expression is valid covers essentially the spontaneous high-injection regime in which our method of evaluating $\tau_{\rm nr}$ operates. This is of importance, since the empirical quantity $\tau_{\rm nr}$ as obtained from our method lumps together all linear loss contributions [cf. Eq. (7)]. This implies that Eq. (8) should be completed with an additional term so as to include the linear leakage losses:

$$\frac{1}{\tau_{\rm nr}} = \frac{1}{\tau_{\rm nr}^b} + \frac{1}{\rm d}[(s_1 + s_2) + v_l] + 2\left(\frac{1}{l} + \frac{1}{b}\right)v, \tag{21}$$

where v_l represents the "effective leakage velocity" defined as

$$v_l \equiv \left(\frac{N'_c}{N_c}\right)\exp\left(\frac{-\Delta E_c}{kT}\right)v'_{\rm diff} = \frac{J_l^{\rm lin}}{qn}. \tag{22}$$

For $n/N_c > 0.5$, the non-negligible fraction of the leakage losses which lies above the broken line in Fig. 1 is not accounted for in the linear recombination term $Vn/\tau_{\rm nr}$ with $\tau_{\rm nr}$ given by Eq. (21). At laser threshold [$n^{\rm th} \simeq 2\times 10^{18}/{\rm cm}^3$ (Refs. 1,2)] this superlinear fraction is dominating by far the linear one.

Apart from the above thermal-emission leakage, another possible leakage phenomenon is the tunneling of electrons to killers situated in the forbidden band gap of the (Ga,Al)As,[16] (or an analogous process of holes at the opposite interface). The contribution of electrons in any infinitesimal energy interval above the GaAs conduction-band minimum to the tunneling process is directly proportional to their density in this interval. As in the spontaneous high-injection regime the Boltzmann approximation applies, any of these interval densities is proportional here to the total density n. Thus the total tunneling losses are also proportional to n over the interval from which $\tau_{\rm nr}$ is evaluated. Conceptually this type of leakage may well be included in the effective interface recombination velocity at the corresponding interface; it is then formally considered as a "quasi-interface recombination" process. A good reason for this concept is the much weaker temperature dependence of both tunneling and recombination as compared to that of the thermal emission.

Just as the losses by thermal-emission leakage, those due to tunneling leakage will also increase strongly superlinearly with n for $n/N_c > 0.5$, owing to Fermi statistics. The superlinear fraction cannot be accounted for by the above concept of quasi-interface recombination.

Summarizing, the presence of leakage losses due to thermal emission and tunneling will show up in the laser threshold current as an additional carrier loss term in excess of the linear recombination term $Vn_{\rm th}/\tau_{\rm nr}$.

III. EXPERIMENTAL

A. Measuring apparatus

The sample is mounted close to a relatively large silicon photodetector wafer. The photons which do not reach this wafer directly are reflected towards it by a hemispherical mirror. The sample, mounted on a holder, fits in a hole through this mirror, while the detector wafer covers the hemisphere like a lid. The product of the transfer and detector efficiencies of this compact combination was found by calibrating with samples having a known external efficiency (determined in an elliptical mirror set up[17]). Using this calibration, the quantity $L_{\rm ext}$ is expressed here as the number of photons which actually leave the laser per second. Thus our $\eta_{\rm ext}$ is what is normally called "the external efficiency", while C is now identical to the light-extraction factor $C_{\rm extr}$. Though basically this calibration is not necessary (cf. the end of Sec. II B), reasonable values of $C_{\rm extr}$ obtained in this way can provide additional confidence in the method.

The values of $L_{\rm ext}$ and $\eta_{\rm ext}$ can be measured automatically at currents of 1, 2, 3, 5, 10, 20, 30, 50, 100, 200, 300, 500,

and 1000 mA. The pulse length is 1 μs. Automatic calculation and plotting of the data in a $1/\eta_{ext}$ vs $1/\sqrt{L_{ext}}$ plot on an XY recorder produces such a plot in a few minutes.

The threshold currents were evaluated from separate L_{ext} vs I measurements, where I was varied continuously (pulse length 0.2 μs). An example is given in the inset of Fig. 6 of Appendix 2.

B. Samples

To illustrate the evaluation method presented in this paper, preliminary results on some thirty samples will be presented. These sample were made from LPE[18] and metal-organic VPE[5] grown GaAs-(Ga,Al)As DH structures. Some of these structures contained Al in the active layer. The samples were selected to cover a wide range of qualities (by which we mean here J_{th}/d values), including very-low-quality far-below-state-of-the-art samples, in order to clearly demonstrate the potentialities of the method.

The active layer was unintentionally n doped for the VPE samples; in some LPE samples it was moderately p doped with Ge. From capacitance-voltage measurements it was found that the net doping concentration N of the active layer was lower than $2\times10^{17}/cm^3$ for all samples. Other

TABLE I. Data of the various samples investigated. The symbols refer to Fig. 3. The $1/\eta_{ext}$ vs $1/\sqrt{L_{ext}}$ plots of sample Nos. 21 and 8 are shown in Fig. 2 and of sample No. 5 in Fig. 6.

No.	Growth No.	Growth method	x_{act} [a] (%)	ΔE_c (eV)	Type [b]	l (μm)	b (μm)	d [c] (μm)	C (%)	τ_{nr} (ns)	J_{th}/d (kA/cm^2 μm)	symbols (see Fig. 3)
1	DHL183	LPE			HM	325	25	0.3*	0.44	10.5	19.9	△
2	DHL183	LPE			HM	325	25	0.3*	0.53	7.9[4]	20.1	
3	DHL272	LPE			HM	300	8	0.3*	1.24	3.0[6]	16.0	□
4	DHS109	LPE	7	0.46	OS	270	50	0.29*	1.23	45.9	5.94	○
5	DHS109	LPE	7	0.46	OS	270	50	0.29*	1.25	29.8	7.39	
6	DHS109	LPE	7	0.46	OS	240	50	0.29*	1.44	33.6	6.25	
7	DHS109	LPE	7	0.46	OS	240	50	0.29*	1.25	33.9	5.65	
8	DHL606	LPE	0	0.430	OS	323	57	0.16	0.55	29.3	7.02	◁
9	DHL606	LPE	0	0.430	OS	330	57	0.16	0.45	29.0	7.36	
10	DHL622	LPE	9	0.436	OS	352	56	0.25	0.35	12.3	9.12	▷
11	DHL622	LPE	9	0.436	OS	352	57	0.28	0.35	14.0	9.73	
12	DHL636	LPE	16	0.367	OS	273	61	0.18	0.69	10.8	11.3	◇
13	DHL636	LPE	16	0.367	OS	273	63	0.16	0.72	10.3	12.8	
14	DHL669	LPE	17	0.352	OS	251	57	0.21	0.31	22.9	10.8	◇
15	DHL606	LPE	0	0.345	BA	302	258	0.2*	0.93	22.7	7.03	▽
16	HDL606	LPE	0	0.345	BA	309	251	0.2*	0.86	21.1	6.05	
17	DHL606	LPE	0	0.345	BA	302	251	0.2*	0.92	23.0	6.65	
18	DHL606	LPE	0	0.345	BA	302	244	0.2*	0.91	24.7	5.43	
19	DHL606	LPE	0	0.345	BA	302	251	0.2*	0.86	18.1	6.44	
20	DHV55	VPE	0	0.399	HM	320	8	0.16*	0.42	0.87[8]	110	▲
21	DHV55	VPE	0	0.399	HM	320	8	0.16*	0.31	0.80[4]	113	
22	DHV290	VPE	0	0.549	OS	302	61	0.39*	0.28	52	13.6	●
23	DHV290	VPE	0	0.549	OS	316	61	0.39*	0.13	53	14.1	
24	DHV290	VPE	0	0.549	OS	316	61	0.39*	0.13	50	15.3	
25	DHV290	VPE	0	0.549	OS	309	61	0.39*	0.13	55	14.4	
26	DHV302	VPE	0	0.499	OS	273	51	0.36	0.44	9.8	10.6	■
27	DHV302	VPE	0	0.499	OS	273	52	0.41	0.41	10.8	10.3	
28	DHV302	VPE	0	0.499	OS	273	51	0.36	0.49	10.6	10.3	
29	DHV319	VPE	0	0.59	OS	316	57	0.30	0.32	31.5	12.2	▼
30	DHV319	VPE	0	0.59	OS	316	57	0.32	0.26	30.9	10.2	
31	DHV319	VPE	0	0.59	OS	320	57	0.32	0.28	19.9	10.8	
32	DHV319	VPE	0	0.59	OS	320	56	0.29	0.38	16.1	12.8	
33	DHV326	VPE	0	0.59	OS	280	57	0.22	0.48	11.7	9.77	◆
34	DHV326	VPE	0	0.59	OS	280	57	0.23	0.42	11.7	10.5	
35	DHV326	VPE	0	0.59	OS	280	57	0.23	0.28	20.7	9.22	

[a] AlAs concentration in the active layer.
[b] HM is high mesa, OS is oxide stripe, and BA is broad area.
[c] The superscript * means that the corresponding value of d represents the average value of a whole wafer rather than the individual value of the sample.

relevant parameters are presented in Table I.

The dimensions l and b were measured by optical means; d was measured using a SEM in the secondary-electron emission mode. In addition to broad-area and high-mesa samples [cf. assumption (1) of Sec. II A] we have also investigated a number of oxide-stripe samples with b between 50 and 65 μm, b means here the width of the oxide stripe. In these samples current spreading occurs. This makes them unsuitable for accurate analysis; the method of taking account of spreading as mentioned at the end of Sec. IV B is not rigorous. The reason for investigating these samples was their standard availability as opposed to broad-area and mesa samples.

IV. EXPERIMENTAL RESULTS AND DISCUSSION

A. The $1/\eta_{ext}$ vs $1/\sqrt{L_{ext}}$ plots and τ_{nr}

Two typical plots are presented in Fig. 2. For both, the expected straight-line behavior can be observed distinctly over an ample interval. Applying Eq. (16), with $B = 10^{-10}$ cm^3/s,[19–21] yields here τ_{nr} values of 0.80 and 29 ns. The values of τ_{nr} for all 35 samples investigated lie between 0.8 and 55 ns (see Table I), which limits are much smaller and larger, respectively, than τ_r^{th} at threshold (see Sec. IV B).

The light-reduction factors lie between the reasonable limits of 0.13 and 1.5% (Table I).

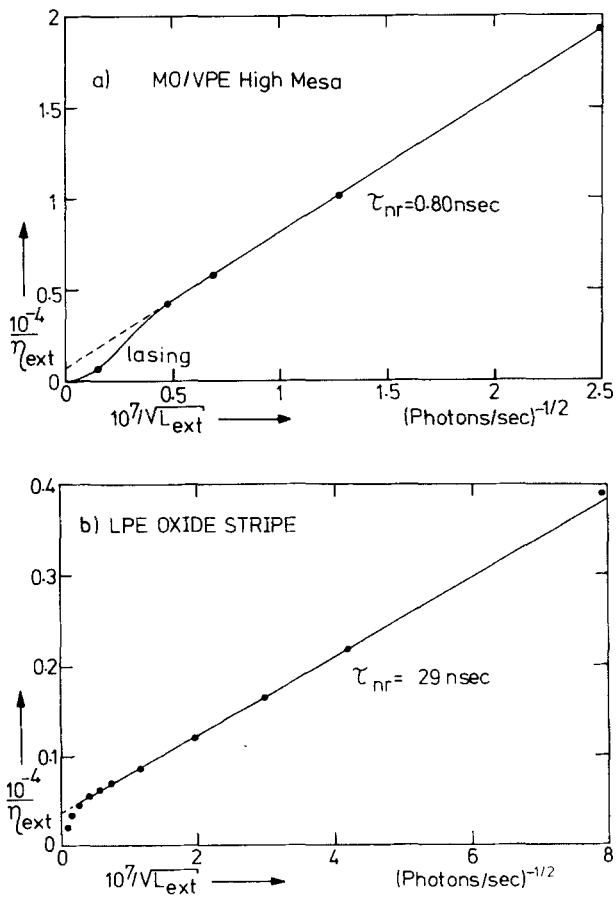

FIG. 2. Plot of reciprocal external quantum efficiency vs reciprocal square root of external photon current for two double-hetero lasers. The values of the effective nonradiative lifetime τ_{nr} as indicated were found from applying Eq. (16) to the slope of the straight line.

In order to quantitatively disentangle the contributions of the three terms in Eq. (8) for the various samples, one has to have samples with different b values made from the same homogeneous wafer, as well as otherwise identical samples with different d values. At the moment we have not yet performed such a systematic study. Nevertheless an interesting conclusion can be drawn concerning the interface recombination velocity s [$\equiv\frac{1}{2}(s_1 + s_2)$]. From Eq. (8) an upper limit for s of a given sample can be found, viz., $d/2\tau_{nr}$. For our best LPE lasers we thus find $s \leqslant 270$ cm/s, whereas for the best VPE lasers $s \leqslant 350$ cm/s.[22]

For the effective recombination velocity v at the outer surfaces, defined by Eq. (5), we can also indicate an upper limit. It follows from the definition of v that $v < v_{diff}$. Using the definitions of v_{diff} and τ_b, given directly after Eq. (5), this can be rewritten as

$$\begin{aligned} v < v_{diff} &= (D_{amb}/\tau^b)^{1/2} \\ &= [2D_h(1/\tau_r + 1/\tau_{nr}^b)]^{1/2} \\ &< [2D_h(1/\tau_r + 1/\tau_{nr})]^{1/2}. \end{aligned}$$

The last expression thus constitutes an upper limit for v. For the samples with $\tau_{nr} \gg \tau_r$ ($\simeq$6 ns at laser threshold, see Sec. IV B) this upper limit amounts to 4×10^4 cm/s.[22]

Further it can be shown that even in our high-mesa samples with $b = 8\,\mu$m the rate of recombination at the outer surfaces is still not the dominating factor. Let h denote that fraction of the total nonradiative recombination rate which is due to recombination at the outer surfaces alone. From Eqs. (6)–(8) it follows that $h \equiv K_s/K = 2v\tau_{nr}/b$, for $b \ll l$. Combining this with the above expression for the upper limit of v one obtains

$$h < (2/b)[2D_h\tau_{nr}(\tau_{nr}/\tau_r + 1)]^{1/2}. \tag{23}$$

Substitution of numerical values for the parameters shows that the highest value of h still lies below 25%, even for the 8-μm-wide high-mesa samples. It should be stressed that in these samples the low value of h is due to the high rates of the other contributions to K given by Eqs. (2) and (4). In fact this was just the reason for fabricating these narrow high-mesa samples, in order to reduce the laser threshold currents to reasonable values. Note further that the quantity h yields a criterion to judge whether there is any possibility of reducing threshold currents by burying the outer surface of a high-mesa laser, e.g., with high-resistivity VPE material.[5]

At high and low currents the experimental $1/\eta_{ext}$ vs $1/\sqrt{L_{ext}}$ plots exhibit deviations from a straight line. The reasons for these deviations are following.

(1) For currents close to and above the laser thresholds the dominating stimulated emission has a considerably higher light-extraction factor than spontaneous emission, owing to the perpendicular incidence of the former on the mirrors. This results in data which lie below the straight line. In principle another effect might also contribute to data lying below that line: photon reabsorption within the active layer will entail an increasing light-extraction factor with increasing η.[23,24] This effect is probably negligible for our small values of d.[21]

A closer inspection of the shape of the curve near laser threshold is presented in Appendix B.

(2) At low currents the line through the data is usually curved upward [see Fig. 2(b); the data for still lower currents, which are not shown here, exhibit much larger upward deviations. The same applies to Fig. 2(a)]. For some samples, on the contrary, downward curvature is observed at lower currents. Both types of curvature occur in the region where the high-injection condition $p \simeq n \gg N$ is no longer fulfilled.

It is easily seen that for any sample in the low-injection regime ($p \ll n = N$ or $n \ll p = N$); η must always approach eventually a constant value; this results in a horizontal asymptote for $1/\eta$ (see Appendix C). Thus it might seem that for any sample the curve should exhibit a continuous downward curvature in going from the sloping to the horizontal asymptote. However, in going to lower injections the effective nonradiative lifetime may decrease considerably below the constant high-injection value τ_{nr}. In these cases an initial upward curvature may be present in going from the straight sloping asymptote to lower injections. It can be shown that such a curvature will be present actually if the ratio of the asymptotic high-injection and low-injection nonradiative lifetimes exceeds the specific value of two.[25] This is treated in detail in Appendix C and represented there in the normalized plot of Fig. 7.

For one of the samples exhibiting upward curvature, viz., No. 11 of Table I, a lifetime ratio was obtained from fitting with the theoretical curves of the above-mentioned plot. The ratio amounted to approximately 50. From this and the corresponding τ_{nr} value of 14 ns a low-injection lifetime follows of roughly only 0.3 ns. The latter value is consistent with an upper limit for the low-injection lifetime of 0.5 ns, obtained from band-gap-luminescence decay measurements on the optically excited remaining part of the same wafer.

B. Type (i) and (ii) losses at laser threshold

We shall make use now of the τ_{nr} values obtained from the $1/\eta_{ext}$ vs $1/\sqrt{L_{ext}}$ plots for estimating the contributions of the type (i) and (ii) losses to the current density at laser threshold. To this end J_{th} is now written as[26]

$$J_{th} = J_1 d/\eta. \tag{24}$$

The exact value of the volume current density J_1 depends on the gain needed to overcome the various optical losses.[26] From the doping concentration and geometry we expect that the gain of all our samples amounts approximately 50 cm^{-1}.[26] This requires for J_1 a value of about 5 $kA/cm^2 \mu m$.[27]

By applying Eq. (10), writing $\tau_r^{th} = 1/Bn_{th}$, and adding the superlinear leakage term at threshold, $J_l^{sup}(n_{th})$, Eq. (24) becomes

$$\frac{J_{th}}{d} = J_1\left(1 + \frac{\tau_r^{th}}{\tau_{nr}}\right) + \frac{J_l^{sup}(n_{th})}{d}. \tag{25}$$

In this equation, τ_{nr} is given by Eq. (21).

For convenience of comparing Eq. (25) with the experimental data, we have plotted the latter in a J_{th}/d vs $1/\tau_{nr}$ plot, see Fig. 3. The line in this plot was obtained from Eq. (25) by substituting $J_1 = 5$ $kA/cm^2 \mu m$ and $J_l^{sup}(n_{th}) = 0$, and by adjusting τ_r^{th} in such way that the line goes through

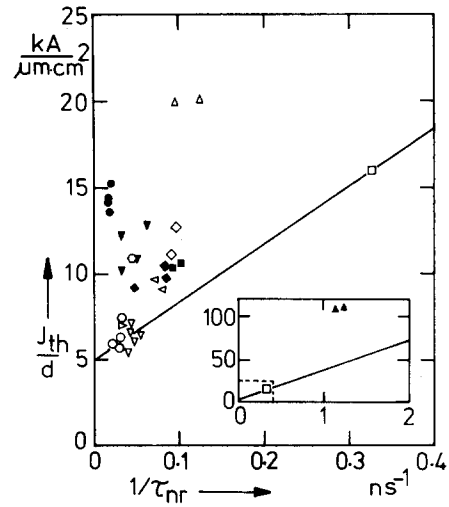

FIG. 3. Plot of laser threshold current density divided by the active-layer thickness vs reciprocal effective nonradiative lifetime for the lasers investigated. The inset shows additional data on a reduced scale. The sloping lines represent Eq. (25) with $J_1 = 5$ $kA/cm^2 \mu m$ and $J_l^{sup}(n_{th}) = 0$. For the meaning of the symbols see Table I.

the two lowest groups of data. This yields a value of τ_r^{th} of 6.7 ns. Since even for the lowest data $J_l^{sup}(n_{th})$ need not be zero exactly, strictly speaking this value of 6.7 ns constitutes an upper limit. The corresponding lower limit for n_{th} equals $1/B\tau_r^{th} = 1.5 \times 10^{18}/cm^3$. An upper limit for n_{th} can be found as follows.

According to Eqs. (7), (10), and (11) the total spontaneous recombination rate at a carrier density n is given by[28]

$$J_{sp}/qd = (1 + 1/Bn\tau_{nr})Bn^2. \tag{26}$$

The laser threshold current density J_{th} will be higher than the value of J_{sp} at laser threshold, owing to the stimulated recombination rate and the leakage losses:

$$J_{th}/qd > (1 + 1/Bn_{th}\tau_{nr})Bn_{th}^2. \tag{27}$$

Substituting the known values of J_{th} and τ_{nr} for a given sample in this equation, the positive root of the corresponding quadratic equation in n_{th} is an upper limit for the n_{th} of the given sample. For the two groups of data through which the line in Fig. 3 was drawn, the upper limits of n_{th} thus obtained equal $1.75 \times 10^{18}/cm^3$ (average value of group ∇) and $1.9 \times 10^{18}/cm^3$, respectively. These values correspond with a lower limit for τ_r^{th} of 5.7 and 5.3 ns, respectively.

The above limits for n_{th} and τ_r^{th} are consistent with the values found before from the line in Fig. 3. Concluding, for these samples one has approximately $n_{th} = 1.7 \times 10^{18}/cm^3$ and $\tau_r^{th} = 6$ ns.

Considering now the whole group of samples, possible differences in optical losses might give rise to differences in n_{th} (and thus in τ_r^{th}). In view of the strong dependence of the gain on n_{th} in the range considered,[13,20] it is reasonable to assume that all our samples have practically the same value of τ_r^{th}. Since the same applies to the value of J_1 in Eq. (25), the vertical distances of the data points above the line in Fig. 3 must be identified with the superlinear leakage-loss term $J_l^{sup}(n_{th})/d$.

In principle, the larger $J_l^{sup}(n_{th})$ values of the data lying above the line compared to those lying near the line in Fig. 3 may arise from various possible factors. Work is in progress, to systematically study the influence of ΔE_c, v'_{diff}, and a graded instead of an abrupt transition from the active to the cladding layer. Grading enables electrons with lower energies to escape from the active layer by penetrating into the graded transition layer and recombining there. Tunneling probabilities through graded instead of abrupt potential barriers are also higher.

Two remarks are due here. First, very high values of $J_l^{sup}(n_{th})$ may entail errors in the evaluation of C and τ_{nr}. This phenomenon as well as means of correcting are treated in Appendix D.

Second, in the oxide-stripe samples of Fig. 3 current spreading presented a problem. From the considerations of Sec. II A it appears that a rigorous treatment is infeasible for this geometry. In the tentative approach followed here the areas used for calculating J_{th} and τ_{nr} of the oxide-stripe samples were determined from optical observation of the light-emitting regions in the spontaneous regime. In the further study, focused on the main causes of leakage losses and on their relation with the phenomenological parameter T_0 defined through $J_{th} \sim \exp(T/T_0)$, only broad-area lasers are being investigated.

V. COMPARISON WITH ALTERNATIVE APPROACHES OF DETERMINING NONRADIATIVE RECOMBINATION LOSSES

In the literature other attempts have already been published to derive information on nonradiative recombination in double-hetero lasers from measurements of light versus current characteristics in the spontaneous regime. The experimental results are generally presented in a double-logarithmic plot of external light intensity versus current. This way of plotting is far less suited for bringing out the characteristic features of the relevant interval. This is demonstrated clearly in Fig. 4. In this figure we present the data of the $1/\eta_{ext}$ vs $1/\sqrt{L_{ext}}$ plot of Fig. 2(b) in the usual way of plotting. In the spontaneous regime this yields a straight line with slope 1.37.

Such a straight or nearly straight line with a slope between 1 and 2 is generally found for the pre-lasing spontaneous regime. This behavior is formally analogous to that of many light-emitting homojunction diodes.[29] For homojunctions in the low-injection regime (below "conductivity modulation") this is attributable to nonradiative recombination in the space-charge region.[30] From the formal analogy in light versus current characteristics the same interpretation is sometimes loosely suggested for lasers.[31] Evidently such an adoption is unjustifiable without a thorough reconsideration of the underlying model for the typical device and the high-injection regime considered here. Apart from that, the approach of expressing firstly the dependence of both the light intensity and the current on the applied voltage, after which this common parameter is eliminated, is less appropriate. It appears from our approach that the carrier density in the active layer is a much more tractable common parameter.

Our method of determining τ_{nr} can further be compared with those based on delay and decay measurements.

In delay measurements the samples are driven into the lasing regime. Therefore leakage losses, which are not accounted for in the usual theory, can lead to considerable underestimation of τ_{nr}. A further disadvantage is the fact that this method is very inaccurate for determining values of τ_{nr} which lie significantly above τ_r. Moreover, many published values are open to doubt in view of the fact that in the simplified model used for interpreting the experimental results the concentration dependence of τ_r has not been taken into account.[32]

Luminescence decay measurements at different current densities J in the spontaneous regime of VPE double-hetero lasers were reported in Ref. 33. The quantity measured in this way is the total lifetime τ given by

$$\frac{1}{\tau} = \frac{1}{\tau_r} + \frac{1}{\tau_{nr}}. \tag{28}$$

From the resulting τ vs J dependence, τ_{nr} was evaluated at 20 ns. This result appears questionable for the following reasons.

(1) Owing to the dependence of τ on n, the decay is nonexponential. This influences the accuracy of the relevant initial slope unfavorably.

(2) In evaluating τ_r and τ_{nr} from the measured τ vs J curve it was assumed that τ_r is proportional to $J^{-1/2}$. This is not correct. From our Eqs. (26) and (28) it can easily be derived that $\tau_r \tau = qd/BJ$. Only for sufficiently high values of J does one have $\tau \simeq \tau_r$, leading to $\tau_r = (qd/BJ_s)^{1/2}$. In the interval considered in Ref. 33, τ_r will vary more strongly with J. [For low values of J one has $\tau_r (\gg \tau_{nr}) \simeq qd/BJ\tau_{nr}$.]

(3) Confirmation of τ_{nr} and τ_r values found from decay was claimed from the good fit between the theoretical light versus current characteristic calculated using these values, and the experimental characteristic. However, the above objection (2) applies here also.

We have replotted the data of the light versus current characteristic from the above work in a $1/\eta_{ext}$ vs $1/\sqrt{L_{ext}}$

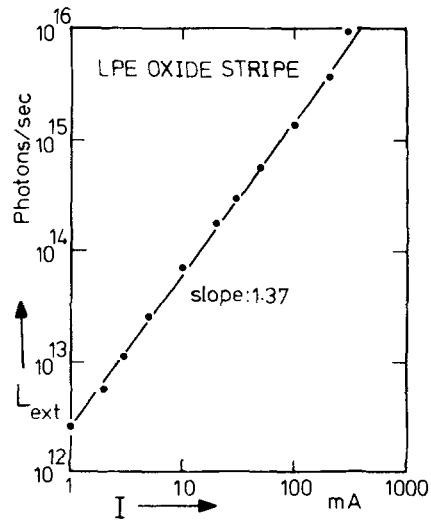

FIG. 4. Double-logarithmic plot of external photon current vs electrical current for the LPE laser of Fig. 2(b).

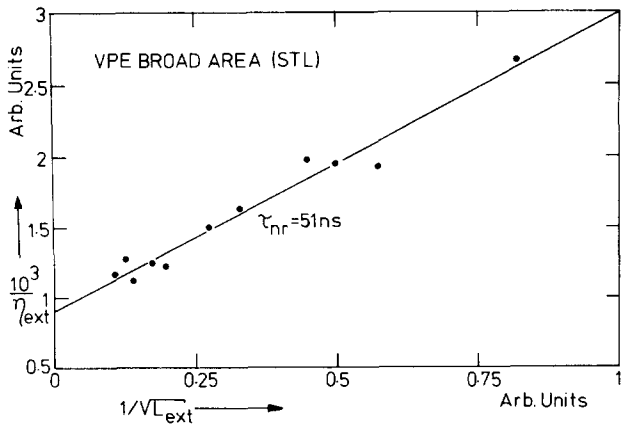

FIG. 5. Data of a laser published in Ref. 33 replotted according to the method developed in the present work (cf. Fig. 2).

plot, see Fig. 5. From this we find a value for τ_{nr} of 51 ns rather than 20 ns. This result entails that the upper limit for the interface recombination velocity s [$\equiv\frac{1}{2}(s_1 + s_2)$] of the samples of Ref. 33, reported to amount to 500 cm/s, is actually as low as 200 cm/s.

Decay measurements for determining τ_{nr} and s of LPE lasers were also reported in Refs. 34 and 35. As the authors recognized, the reported values of s may be considerably larger than the saturated values at laser operation. This is concluded from the convexity of the semilogarithmic decay curves of the relevant samples, indicating the occurrence of killer saturation phenomena. Occurrence of saturation is consistent with the manifest tendency of the evaluated s values to decrease with increasing active-layer thickness d as observed in Figs. 2–4 of Ref. 35: an increase of d entails an increase of the excited carrier density n, which tends to saturate interface killers. Quantitatively an increase of n with increasing d can be seen from considering stationary excitation with homogeneous excitation density g: for dominating interface recombination this yields according to Eq. (8) $n = g\tau_{nr} \simeq gd/2s$ for small values of d. The actual increase of the average n with d will be sublinear owing to the decrease of generation density with depth. This makes the observed decrease of s all the more significant. Thus the lowest value of s reported, viz., 250 cm/s, may still lie considerably above the completely saturated value as determined with our method.

VI. CONCLUSIONS

The method presented yields a simple, fast and accurate means for determining the internal quantum efficiency and the high-injection nonradiative carrier lifetime τ_{nr} of double-hetero lasers and LED's with net doping concentrations in the active layer below $10^{18}/cm^3$. The quantity τ_{nr} thus evaluated lumps together the effects of all nonradiative recombination processes taking place in the bulk of the active region, at its interfaces and at its outer surfaces [cf. Eq. (8)]. Each of these contributions is characterized by a specific parameter, viz., the bulk nonradiative lifetime τ_{nr}^b, the interface recombination velocities s_1 and s_2, and the effective outer-surface recombination velocity v. It is important that our method yields the value of the lifetime in the high-injection regime ($p \simeq n$). This implies that all aforementioned recombination mechanisms are operating in the saturated-killer regime, so that the corresponding specific parameters and the overall τ_{nr} are essentially constant (i.e., independent of n). This constant high-injection value τ_{nr} is exactly the value figuring in the expression for the laser threshold current density J_{th} [Eq. (25)].

The knowledge of τ_{nr} can be used for diagnosing high values of J_{th}. From an analysis of possible carrier-leakage contributions to J_{th} it turned out that these will also contribute to τ_{nr} [second term between square brackets in Eq. (21)]. However, during lasing it is only a small fraction of the total leakage which does manifest itself in τ_{nr}, viz., the fraction which is directly proportional to the carrier density n in the active layer. The much larger superlinear part appears as a separate additional current term in Eq. (25) for J_{th}. The accuracy with which the high-injection lifetime τ_{nr} can be determined now allows the attribution of the "excess" electrical losses (i.e., those not attributable to τ_{nr}) to superlinear carrier losses. Since Auger losses are unlikely to contribute significantly at the carrier concentrations in question, the excess superlinear losses can be identified with leakage losses.

Our method yields more reliable τ_{nr} values than those based on delay and decay measurements. Published values of the effective nonradiative lifetime evaluated from decay measurements are lower than the saturated high-injection values. This implies that the inferred values of the interface recombination velocities s [$\equiv\frac{1}{2}(s_1 + s_2)$] represent an overestimation for the high-injection regime.[33,34] The present method yields the correct high-injection values.

An interesting point is that our approach enables the internal quantum efficiency (at different currents) to be determined from measurements of the external efficiency vs current expressed in completely arbitrary units. To this end there is no need to measure the light-extraction factor (i.e., the ratio between external and internal quantum efficiencies). Just the reverse, if required, the method may be used for the determination of this factor.

Finally it has been shown (see Appendix C) how from an extension of the measurements to lower-injection conditions additional information characterizing the dominant killers may be obtained, viz., the ratio of the hole and electron capture coefficients.

APPENDIX A: CONDITIONS FOR HOMOGENEOUS $p \simeq n$

In this appendix we shall discuss the conditions for homogeneous carrier distributions in the active region in the high-injection regime, as mentioned briefly under point (3) of Sec. II A.

(1) We consider first the conditions for absence of concentration variations perpendicular to the interfaces. The first, obvious condition requires that $d \ll L_{amb}$. By definition we have $L_{amb} \equiv (D_{amb}\tau^b)^{1/2}$, where $D_{amb} = 2D_h D_e/(D_h + D_e) \simeq 2D_h$ (if $D_h \ll D_e$), and where $1/\tau^b = 1/\tau_r + 1/\tau_{nr}^b$; here τ_r is the radiative lifetime and τ_{nr}^b the bulk nonradiative lifetime. According to Eq. (8) one has

$\tau_{nr}^{b} > \tau_{nr}$, where τ_{nr} is the effective nonradiative lifetime as determined with our method. After substitution of this all, and using $D_h = \mu_h kT/q$, we find that

$$L_{amb} > [(2\mu_h kT/q)/(1/\tau_r + 1/\tau_{nr})]^{1/2}.$$

For the samples investigated here one has $\mu_h \simeq 200$ $cm^2/V\,s$.[36] Using our values of τ_r and τ_{nr} (see Table I), we find that $d/L_{amb} < 0.18$ for all our samples.

A second, less obvious condition for absence of concentration gradients perpendicular to the interfaces is that $s_1 + s_2 \ll 8D_h/d$.[3] Since it follows from Eq. (8) that $s_1 + s_2 < d/\tau_{nr}$, this condition is fulfilled when $8D_h\tau_{nr}/d^2 \gg 1$. The minimum value of $8D_h\tau_{nr}/d^2$ for our samples turns out to be 125.

(2) Owing to recombination at the outer surfaces, a layer of reduced carrier concentrations will extend over a depth of roughly L_{amb} from these surfaces. These layers constitute a negligible fraction of the total active region V if $2L_{amb}/b \ll 1$. The ratio $2L_{amb}/b$ is roughly 0.3 for our high-mesa samples with $b = 8\ \mu m$, of the order of 0.1 for the oxide-stripe samples and for the high-mesa samples with $b = 25\ \mu m$, and of the order of 0.02 for the broad-area samples.

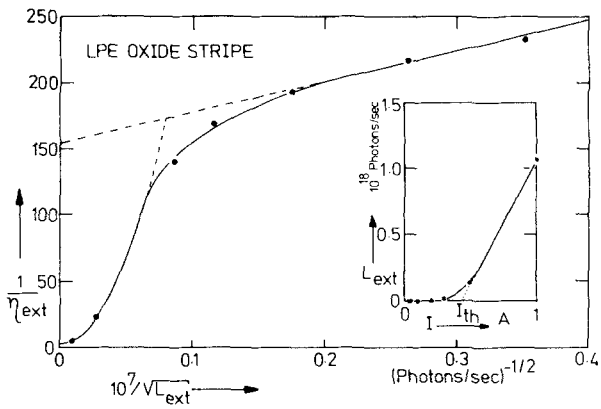

FIG. 6. Example of change-over from spontaneous emission to laser regime, in an expanded plot made according to the method developed in the present work (cf. Figs. 2 and 5). The inset shows the usual way of plotting for evaluating the laser threshold current I_{th}, and the differential quantum efficiency η_{diff} which equals the slope of the straight line. This straight line corresponds to the parabola in the main figure. (The data points in the inset correspond with those in the main figure; the continuous curve in the inset was obtained from the separate method described at the end of Sec. III A).

APPENDIX B: INFLUENCE OF LASING ON THE SHAPE OF THE $1/\eta_{ext}$ VS $1/\sqrt{L_{ext}}$ CURVE

The data near and above laser threshold lie below the extrapolated straight line of the spontaneous high-injection regime. This is due to the much larger light-extraction factor of the stimulated emission. In this interval the curve approximates asymptotically to a parabola. This is seen as follows. Let us write

$$\frac{1}{\eta_{ext}} \equiv \frac{I}{qL_{ext}} = \frac{I - I_{th}}{qL_{ext}} + \frac{I_{th}}{qL_{ext}}. \tag{B1}$$

From the usual L_{ext} vs I plot it turns out that the quantity $(I - I_{th})/qL_{ext}$ generally becomes practically constant for I sufficiently above I_{th}. Denoting this value as η_{diff},[37] Eq. (B1) becomes

$$\frac{1}{\eta_{ext}} = \frac{1}{\eta_{diff}} + \frac{I_{th}}{q(\sqrt{L_{ext}})^2}. \tag{B2}$$

In Fig. 6 this parabola is shown for one sample. The values of the parameters η_{diff} and I_{th} used for calculating this parabola were derived from the corresponding L_{ext} vs I plot (see inset). In analogy with the straight-line interval [Eq. (15)], extrapolation of the parabola to $1/\sqrt{L_{ext}} = 0$ yields here the light-extraction factor for the lasing regime, i.e., η_{diff}.

APPENDIX C: THE SHAPE OF THE $1/\eta_{ext}$ VS $1/\sqrt{L_{ext}}$ CURVE BELOW THE HIGH-INJECTION REGIME

In Sec. II A it has been shown that in the high-injection regime ($p \simeq n \gg N$) the effective nonradiative lifetime is always constant, i.e., independent of n, owing to saturation of all killers. At lower injections, where the killers are not (completely) saturated, the lifetime may be considerably lower and vary with n. In this appendix we shall examine the influence of this effect on the shape of the $1/\eta_{ext}$ vs $1/\sqrt{L_{ext}}$ curve. Assuming a constant light-extraction factor throughout the whole spontaneous emission regime, this shape will be analogous to that of the "internal" $1/\eta$ vs $1/\sqrt{L}$ curve. Thus we need only consider here the latter.

For any laser, at sufficiently low currents the $1/\eta$ vs $1/\sqrt{L}$ curve will tend eventually to a horizontal asymptote. This is seen as follows. We consider an n-type active layer. In the low-injection regime ($p \ll n = N$) Eq. (10) should be replaced by $L = BVpn$. In Eq. (7), τ_{nr} should be replaced by its low-injection counterpart; this is the effective nonradiative minority-carrier (here:hole) lifetime τ_h. This yields $K = Vp/\tau_h$. From the modified equations for K and L, instead of Eq. (12) one finds

$$\frac{1}{\eta} = 1 + \frac{K}{L} = 1 + \frac{1}{BN\tau_h}, \tag{C1}$$

which is constant.

In the following it will be assumed that only a single type of bulk or interface killer contributes to τ_h and τ_{nr}. According to Eq. (3) one can then write for the effective high-injection τ_{nr}:

$$\tau_{nr} = \tau_h + \tau_e. \tag{C2}$$

In cases where $\tau_e \ll \tau_h$ one has $\tau_{nr} \simeq \tau_h$: the effective lifetimes in the high- and low-injection regimes are equal. There are no saturation effects in these cases, because the bottleneck for recombination remains hole capture even for equal hole and electron concentrations. The transition in going from the high- to the low-injection regime, i.e., from the sloping asymptote given by Eq. (12) to the horizontal asymptote given by Eq. (C1), results then in a convex curve (see bottom curve in Fig. 7).

The general shape of the curve (without the above restriction $\tau_e \ll \tau_h$) can be found as follows. For arbitrary n one has $n = p + N$, when the charge on the killer centers is negligible. Equation (10) then becomes

$$L = VBpn = VBp(p + N). \tag{C3}$$

The corresponding generalization for K is found by replac-

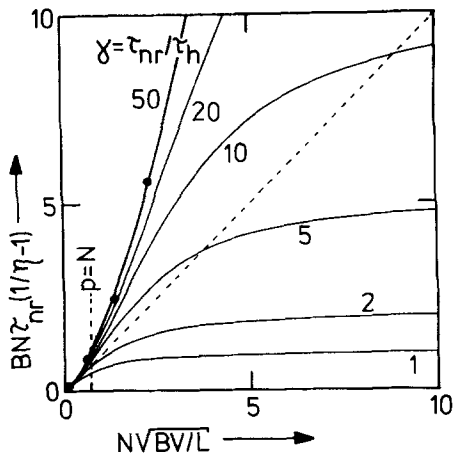

FIG. 7. The $1/\eta$ vs $1/\sqrt{L}$ curves in normalized form, extended to the low-injection regime. These curves are fully characterized by the single parameter γ, which depends only on the ratio of the hole and electron capture coefficients of the relevant killers ($\gamma = 1 + c_h/c_e$). Vertical lines in this diagram correspond to constant values of p/N. The line for $p/N = 1$, which bounds the high-injection regime, is indicated. For the experimental data points, see text at the end of Sec. IV A.

ing τ_{nr} in Eq. (7) by the general expression[4]

$$\tau_{gen} = \frac{p\tau_{nr} + N\tau_h}{p + N}. \tag{C4}$$

This yields

$$K = \frac{Vp(p+N)}{p\tau_{nr} + N\tau_h}. \tag{C5}$$

Using Eqs. (C3) and (C5) we find, for $1/\eta$,

$$\frac{1}{\eta} = 1 + \frac{K}{L} = 1 + \frac{1}{B(p\tau_{nr} + N\tau_h)}. \tag{C6}$$

It turns out to be more tractable if this is rewritten in the following dimensionless form:

$$Y \equiv BN\tau_{nr}\left(\frac{1}{\eta} - 1\right) = \frac{1}{p/N + \tau_h/\tau_{nr}}. \tag{C7}$$

From Eq. (C3) the following dimensionless relation can be derived:

$$X \equiv N(BV/L)^{1/2} = \frac{1}{[(p/N)(1+p/N)]^{1/2}}. \tag{C8}$$

The shape of the $1/\eta$ vs $1/\sqrt{L}$ curve is fully reflected in a plot of Y vs X. Such a plot is found from eliminating p/N from Eqs. (C7) and (C8).

In Fig. 7 the resulting curves are presented for different values of the parameter

$$\gamma \equiv \tau_{nr}/\tau_h = 1 + \tau_e/\tau_h. \tag{C9}$$

At the origin all curves start with the same slope of unity. The horizontal asymptotes lie at a height $Y = \gamma$. The curves for $\gamma \leqslant 2$ lie completely below the sloping asymptote, those for $\gamma > 2$ lie partially above it. The latter curves exhibit a slightly concave interval, a point of inflection, and a point of intersection with the sloping asymptote. It can easily be proved now that the value $\gamma = 2$ represents exactly the demarcation between the two families of curves. The value of p/N at the point of intersection between a YX curve and the asymptote $Y = X$ follows from equating the right-hand sides of Eqs. (C7) and (C8). This yields $p/N = 1/\gamma(\gamma - 2)$; only for $\gamma > 2$ this does give a positive value for the point of intersection.

The value $\gamma = 2$ or $\tau_e = \tau_h$ thus represents the demarcation between the families of curves with opposite deviations near $p = N$ from the high-injection straight sloping asymptote in the Y vs X, $1/\eta$ vs $1/\sqrt{L}$, and $1/\eta_{ext}$ vs $1/\sqrt{L_{ext}}$ plots. When bulk killers are dominating the nonradiative recombination, the condition $\tau_e = \tau_h$ can be rewritten as $c_h = c_e$ [cf. Eq. (3)]. When interface recombination is dominating, exactly the same equality applies for the hole and electron recombination coefficients of the interface killers. The upward or downward curvature of experimental curves beyond the straight-line interval thus yields a direct criterion for c_h/c_e of the dominating killers being larger or smaller than unity, respectively. A more precise determination of c_h/c_e may be obtained from a fitting procedure. Note that no knowledge of N is needed for evaluating $\gamma \equiv 1 + c_h/c_e$ from a fit. Obviously, fitting even becomes superfluous if one can measure the curve down to sufficiently low efficiencies. This would yield directly the value of τ_h from the measured asymptote [Eq. (C1) with (14)]. For this, knowledge of N is needed. From τ_h and τ_{nr} the value of $c_h/c_e (= \tau_{nr}/\tau_h - 1)$ then follows.

Note that for lasers with a p-type active layer τ_e in all equations should be replaced by τ_h, and vice versa. Thus, for example, γ of Eq. (C9) will become $\gamma \equiv \tau_{nr}/\tau_e = 1 + \tau_h/\tau_e$. This implies that, if the same type of killers dominates in lasers with n- and p-type active layers, the corresponding $1/\eta_{ext}$ vs $1/\sqrt{L_{ext}}$ curves near $p = N$ will deviate in opposite senses from the sloping asymptote.

The evaluation of the characteristic ratio $c_h/c_e (= 1 - \gamma)$ as presented in this appendix may be of use in identifying the dominant killers.

APPENDIX D: INFLUENCE OF LEAKAGE ON EVALUATION OF C AND τ_{nr}

The value of τ_{nr} as evaluated with the aid of Eq. (16) lumps together all linear loss contributions; this is expressed by Eq. (21), in which the linear leakage term v_l/d has been included. In case of thermal emission over an abrupt barrier followed by diffusion, v_l equals the reduced diffusion velocity in the cladding layer as defined by Eq. (22). Physically the linear term corresponds with the Boltzmann approximation of the Fermi distribution, see Fig. 1.

Actually the linear term represents the first of a power-series expansion of n' in n. The coefficients of the higher-order terms follow from the series expansion[38]

$$\exp(\epsilon) = F_{1/2}(\epsilon) + \tfrac{1}{4}(\sqrt{2})F_{1/2}^2(\epsilon) + \cdots, \tag{D1}$$

which, according to Eqs. (17) and (18) can be considered as a normalized power-series expansion of n' in n. For high leakage losses, the quadratic term in Eq. (D1) may produce errors in the values of the light-extraction coefficient and the nonradiative lifetime as determined with our method. This is seen as follows.

Using Eq. (D1) together with Eqs. (17) and (18), the total leakage loss term per unit of area can be expressed as

$$J_l^{\rm tot}/q = (J_l^{\rm lin} + J_l^{\rm sup})/q = n' v'_{\rm diff} = v_l\{n + [\tfrac{1}{4}(\sqrt{2})/N_c]n^2 + \cdots\}, \quad \text{(D2)}$$

where v_l is defined by Eq. (22). Multiplying this expression by the area bl, adding the linear and quadratic terms to the right-hand side of Eq. (11), and following further the same procedure which led to Eq. (15), we arrive at the modified equation

$$\frac{1}{\eta_{\rm ext}} = \frac{1}{C}\left[1 + \frac{\tfrac{1}{4}\sqrt{2}}{N_c}\frac{v_l}{Bd}\right] + \frac{1}{\tau_{\rm nr}}\left(\frac{V}{BCL_{\rm ext}}\right)^{1/2}. \quad \text{(D3)}$$

The quantity $\tau_{\rm nr}$ in this equation is defined again by Eq. (21) with (22).

From Eq. (D3) it is seen that the quadratic term of Eq. (D2) disturbs the linear relation between $1/\eta_{\rm ext}$ and $1/\sqrt{L_{\rm ext}}$ no more than the linear term did. Consequently, extrapolation of the linear interval to $1/\sqrt{L_{\rm ext}} = 0$ yields an apparent reduction factor C' which is smaller than the actual value C:

$$\frac{1}{C'} = \frac{1}{C}\left(1 + \frac{\tfrac{1}{4}\sqrt{2}}{N_c}\frac{v_l}{Bd}\right). \quad \text{(D4)}$$

An estimation of the error for a given sample can be made by rewriting the second term between parentheses. Using Eq. (22) one can write

$$\left[\frac{\tfrac{1}{4}(\sqrt{2})}{N_c}\right]\left(\frac{v_l}{Bd}\right) = \left(\frac{\tfrac{1}{4}(\sqrt{2})}{N_c Bnq}\right)(J_l^{\rm lin}/d).$$

The value of this expression can be found after substituting for n and $J_l^{\rm lin}$ the values at laser threshold. Doing so, and expressing $J_l^{\rm lin}(n_{\rm th})$ in $J_l^{\rm sup}(n_{\rm th})$ by making use of Eqs. (22) and (D2), the ratio C/C' given by Eq. (D4) can be rewritten as

$$\frac{C}{C'} = 1 + \frac{\tfrac{1}{4}\sqrt{2}}{N_c B n_{\rm th} q} \times \left[\left(\frac{\tfrac{1}{4}\sqrt{2}}{N_c}\right)n_{\rm th} + \left(\frac{\tfrac{1}{4} - (1/9)\sqrt{3}}{N_c^2}\right)n_{\rm th}^2 + \cdots\right]^{-1} \times \frac{J_l^{\rm sup}(n_{\rm th})}{d}. \quad \text{(D5)}$$

Substituting the values for GaAs ($N_c = 4.3\times10^{17}\ {\rm cm}^{-3}$, $n_{\rm th} = 1.7\times10^{18}\ {\rm cm}^{-3}$, $B = 10^{-10}\ {\rm cm}^3\ {\rm s}^{-1}$), Eq. (D5) becomes

$$\frac{C}{C'} = 1 + \frac{0.1 J_l^{\rm sup}(n_{\rm th})}{d}, \quad \text{(D6)}$$

where $J_l^{\rm sup}(n_{\rm th})/d$ is expressed in kA/cm^2 μm. The value of the last quantity equals the vertical distance of the data point considered above the sloping line in the $J_{\rm th}/d$ vs $1/\tau_{\rm nr}$ plot of Fig. 3. For most of our samples this value is equal to or lower than 4 kA/cm^2 μm, corresponding with a relative error in C of 30% or less.

Evidently, substitution of C' rather than C in Eq. (16) will yield an apparent $\tau'_{\rm nr}$ which is larger than $\tau_{\rm nr}$:

$$\tau'_{\rm nr}/\tau_{\rm nr} = (C/C')^{1/2}. \quad \text{(D7)}$$

For the above numerical example, the relative error in $\tau_{\rm nr}$ is 18% or less.

An obvious method of improving the accuracy for samples with large leakage losses consists in correcting the value of $\tau'_{\rm nr}$ with the aid of Eq. (D7); eventually this can be followed by iterating the procedure using this corrected value, starting with reading a new value of $J_l^{\rm sup}(n_{\rm th})/d$ from the $J_{\rm th}/d$ vs $1/\tau_{\rm nr}$ plot.

ACKNOWLEDGMENTS

The authors are greatly indebted to P. J. J. Eijmberts for skillfully designing and realizing the apparatus for the $1/\eta_{\rm ext}$ vs $1/\sqrt{L_{\rm ext}}$ measurements. They wish to thank W. J. Leswin, W. Nijman, A. G. M. de Nijs, and H. Veenvliet for growing the laser structures, and G. L. Dinghs for the laser fabrication. Thanks are due to W. J. A. Schoenmakers and A. M. E. Willekes for laser threshold current measurements, to J. A. de Poorter for SEM measurements, and P. J. de Waard and H. Veenvliet for comments.

[1] H. C. Casey, Jr. and M. B. Panish, *Heterostructure Lasers*, p. 228, part B (Academic, New York, 1978).
[2] H. Kressel and J. K. Butler, *Semiconductor lasers and heterojunction LEDs* (Academic, New York, 1977), p. 259.
[3] C. van Opdorp and H. Veenvliet, IEEE J. Quantum Electron. **QE-15**, 817 (1979).
[4] J. S. Blakemore, *Semiconductor Statistics* (Pergamon Press, Oxford, 1962), p. 270.
[5] H. Veenvliet, C. van Opdorp, R. P. Tijburg, and J. P. André, IEEE J. Quantum Electron. **QE-15**, 762 (1979).
[6] Suppose that even the saturated s_r is still much larger than $v_{\rm diff}$, so that $v \simeq v_{\rm diff} = (2D_h/\tau^b)^{1/2}$. The total bulk lifetime $\tau^b \equiv (1/\tau_r + 1/\tau_{\rm nr}^b)^{-1}$ will vary with a gradient in n, so that in this case $v_{\rm diff}$ is not constant in the layer of reduced n. However, since the variation in $v_{\rm diff}$ will be considerably smaller than that in τ^b, it is reasonable to assume that Eq. (6) with a constant v still applies here approximately if an appropriate average value of $v_{\rm diff}$ is chosen.
[7] Equation (10) can be derived by straightforward application of the mass-action law, using $p = n$. This procedure is justified in the regime where neither of the two quasi-Fermi levels moves into the corresponding band.[8,9] This covers essentially the regime where spontaneous dominates stimulated recombination.
[8] G. H. B. Thompson, *Physics of semiconductor laser devices* (Wiley, Chichester, 1980), p. 77.
[9] P. T. Landsberg, Proc. Phys. Soc. London Sec. B **70**, 282 (1957).
[10] E. Burstein, Phys. Rev. **93**, 632 (1954).
[11] R. K. Willardson and Albert C. Beer, *Semiconductors and semimetals* (Academic, New York, 1966), see contribution M. Gershenzon, p. 289.
[12] From Stern's plot of the net absorption coefficient versus photon energy for different values of n,[13] it appears that there is already significant contribution of stimulated recombination for $n \simeq 10^{18}\ {\rm cm}^{-3}$. Such a contribution will produce an increase of C. However, Stern's calculation was done for a p-type active layer with an equilibrium hole concentration of $1.2.\times10^{18}\ {\rm cm}^{-3}$. For our samples, which are either low-doped p type or unintentionally doped n type, the first appearance of an energy interval of positive gain will be shifted to higher values of n.
[13] See Ref. 1, part A, p. 164.
[14] Chii-Ming Wu and Edward S. Yang, J. Appl. Phys. **49**, 3114 (1978).
[15] In contrast with the recombination velocities at the interfaces and possibly at the outer surfaces, the diffusion velocity $v'_{\rm diff}$ will not be reduced by saturation effects. The reason is that n' is much smaller than the dope concentration in the (Ga,Al)As layer.
[16] W. T. Tsang, Appl. Phys. Lett. **33**, 245 (1978).
[17] J. A. W. van der Does-de Bye, Rev. Sci. Instrum. **40**, 320 (1969).
[18] G. A. Acket, J. J. Daniele, W. Nijman, R. P. Tijburg, and P. J. de Waard, Philips Tech. Rev. **36**, 190 (1976).
[19] F. Stern, IEEE J. Quantum Electron. **QE-9**, 290 (1973).
[20] F. Stern, J. Appl. Phys. **47**, 5382 (1976).

[21]R. J. Nelson and R. G. Sobers, J. Appl. Phys. **49**, 6103 (1978).
[22]In Ref. 5 a rough value of $s \simeq 2 \times 10^4$ cm/s was reported for our MO-VPE lasers. This value appears now to be a high overestimation, since the then neglected considerable leakage current was attributed wrongly to interface recombination. For the same reason the value of v reported in Ref. 5 may be much too high.
[23]T. Kuriyama, T. Kamiya, and M. Yanai, Jpn. J. Appl. Phys. **16**, 465 (1977).
[24]K. Mettler, Phys. Status Solidi A **49**, 163 (1978).
[25]Upward curvature in many narrow-stripe lasers with $b = 10\,\mu$m (not further reported on here) even turned out to totally obscure the straight-line interval. This is, however, mainly due here to volume contraction of the active region with increasing current: from Eq. (15) it is seen that decrease of V and increase of τ_{nr} will exert the same type of influence on the shape of the characteristics.
[26]H. C. Casey, Jr. and M. B. Panish, *Heterostructure Lasers* (Academic, New York, 1978), part A, p. 183.
[27]See Ref. 8, p. 89.
[28]Equation (26) can also serve to check that for a given sample the high-injection condition $p \simeq n \gg N$ is really satisfied over the whole observed straight-line interval in the $1/\eta_{ext}$ vs $1/\sqrt{L_{ext}}$ plot. Substituting for J_{sp} the lowest current density value in this interval, the corresponding value of n is the lowest there. The value of n thus calculated for our samples all fulfill the high-injection condition. On the other hand, quite analogously, one can calculate the highest value of n in the observed straight-line interval by substituting for J_{sp} the highest current density value in that interval. This yields a rough average value of 10^{18} cm^{-3} for our samples. Thus the straight-line interval appears to extend a bit further than the expected limit both for the validity of Boltzmann Eq. (10) and for the negligibility of superlinear leakage losses J_i^{sup}. Among others, this might be attributable to partial mutual compensation of opposed effects: a non-negligible J_i^{sup} and a decrease of B,[20] on the one hand, against an increase of the light-reduction factor C, due to the contribution of stimulated recombination (superradiance) on the other.
[29]A. A. Bergh and P. J. Dean, *Light-emitting diodes* (Clarendon, Oxford, 1976), p. 395.
[30]C. T. Sah, R. N. Noyce, and W. Shockley, Proc. IRE **45**, 1228 (1957).
[31]See Ref. 2, p. 70.
[32]R. W. Dixon and W. B. Joyce, J. Appl. Phys. **50**, 4591 (1979).
[33]E. J. Thrush, P. R. Selway, and G. D. Henshall, Electron. Lett. **15**, 156 (1979).
[34]R. J. Nelson and R. G. Sobers, Appl. Phys. Lett. **32**, 761 (1978).
[35]R. J. Nelson, J. Vac. Sci. Technol. **15**, 1475 (1978).
[36]W. von Münch, *Technologie der Galliumarsenid-Bauelemente* (Springer, Berlin, 1969), p. 12.
[37]See Ref. 26, p. 180.
[38]W. B. Joyce and R. W. Dixon, Appl. Phys. Lett. **31**, 354 (1977).